

# Identifying drivers of energy resolution variation in a multi-KID phonon-mediated detector

K. Ramanathan · T. Aralis · R. Basu Thakur · B. Bumble · Y.-Y. Chang · O. Wen · S. R. Golwala

Received: 11/01/2021

**Abstract** Phonon-mediated particle detectors employing Kinetic Inductance Detectors (KIDs) on Silicon substrates have demonstrated both  $O(10)$  eV energy resolution and mm position resolution, making them strong candidates for instrumenting next generation rare-event experiments such as in looking for dark matter and for neutrino measurements. Previous work has demonstrated the performance of an 80-KID array on a Si wafer, however current energy resolution measurements show a  $\sim 25\times$  difference between otherwise identical KIDs – between 5 to 125 eV on energy absorbed by the KID. Here, we use a first principles approach and attempt to identify the drivers behind the resolution variation. In particular, we analyze a subset of 8 KIDs using the unique approach of pulsing neighboring KIDs to generate signals in the target. We tentatively identify differences in quality factor terms as the likely culprit for the observed variation.

**Keywords** Kinetic Inductance Detector (KID), Athermal phonon, Energy resolution, Low energy detector

## 1 KID Based Phonon Mediated Detectors

Kinetic Inductance Detectors, as first proposed by Day et al. [1], are excellent devices to instrument rare-event search experiments due to their low energy threshold, inherent multiplexability, and straightforward cryogenic RF readout. Previous work by Moore et al. [2] has demonstrated how patterning 20 KID resonators on a  $4\text{ cm}^2$  Silicon substrate enabled both  $\mathcal{O}(100)$  eV energy and sub-mm position reconstruction of external radiation incident on the detector. Interacting particles within the bulk produce an athermal phonon population, which propagate to the surface KID film and effect a change in the quasiparticle density of the superconducting material by breaking Cooper pairs. The subsequent modified non-linear kinetic inductance then modulates the RF transmission properties of the resonator

---

K. Ramanathan · T. Aralis · R. Basu Thakur · Y.-Y. Chang · S. R. Golwala  
Division of Physics, Mathematics, & Astronomy, California Institute of Technology, Pasadena, CA 91125, USA  
E-mail: karthikr@caltech.edu

B. Bumble  
Jet Propulsion Laboratory, Pasadena, CA 91107, USA

and by measuring said transmission (and in conjunction with Mattis-Bardeen (M-B) theory) allows one to work back through the chain to figure out details of the original energy deposit. Subsequent work by Chang et al. [3] led to the fabrication of an 80-KID device on a 75 mm diameter  $\times$  1 mm thick Si substrate, as seen in Fig. 1, operated at 60 mK in an Oxford Kelvinox 25 dilution refrigerator. This prototype detector couples all KIDs to a single 300 nm wide coplanar waveguide (CPW) Niobium ( $\Delta = 1.5$  meV superconducting gap) feedline. The capacitive and inductive elements are made of Aluminium ( $\Delta = 200 \mu\text{eV}$ ). The resonators are intentionally over-coupled, with the capacitive quality factor  $Q_c$  smaller than the intrinsic quality factor  $Q_i$  so as to allow recovery of the phonon rising edge information. All KIDs are nominally identical other than small changes in the inductor length to separate their resonant frequencies by O(MHz) in the 3.05–3.45 GHz band. KID output is fed to a cryogenic HEMT amplifier with a 3 K noise temperature and data is finally acquired using an Ettus Research SDR. As designed the expected deposited energy resolution  $\sigma_E$  of the detector is  $< 20$  eV across all KIDs.

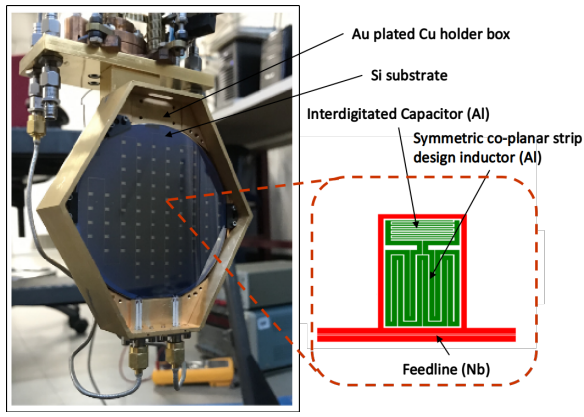


Fig. 1: 80 KID device on a 3 in, 1 mm thick Si. substrate, mounted in a Gold plated Copper box. Cartoon zoom of a single resonator element, showing 300 nm Niobium feedline coupled to Aluminium KID composed of an interdigitated capacitor and meandering symmetric coplanar inductor.

## 2 Energy resolution estimation

The energy resolution can be estimated using a novel in-array technique without use of a known energy external radiation source. By pulsing a source KID with large readout power, one creates a non-equilibrium quasiparticle population within the device. Recombination then generates phonons that propagate out into the substrate. These are then absorbed by other target KIDs, like a regular particle interaction. Fig. 2 details this process and one can see the response of neighboring KIDs to a square  $20 \mu\text{s}$  square pulse. We can then apply an optimal filter (OF) estimate for the resolution [4] given by:

$$\sigma^2 = \frac{\int_{-\infty}^{\infty} df J(f) \left| \frac{\bar{s}(f)}{J(f)} \right|^2}{\left[ \int_{-\infty}^{\infty} df \frac{|\bar{s}(f)|^2}{J(f)} \right]^2} \quad (1)$$

where  $\tilde{s}$  is Fourier transform of a pulse signal time stream and  $J$  is the power spectral density of a corresponding noise stream. For the analysis presented here we selected a subset of 8 resonators on the prototype device, chosen to be neighbors in frequency space from 3130–3170 MHz, and took 2 data runs — a series of pulses applying  $>10$  dBm to neighboring resonators, and corresponding noise time streams, taken over readout powers ranging from -25 dBm to -7 dBm. General analysis and processing details can be found in e.g. Ref. [5]. Applying the OF framework shows large variation in measured energy resolution — the best performing KIDs hit the design goal of  $\sigma_E < 20$  eV while the worst performing devices have  $\sigma_E > 100$  eV. This variation is not explicable under an amplifier-limited noise model.

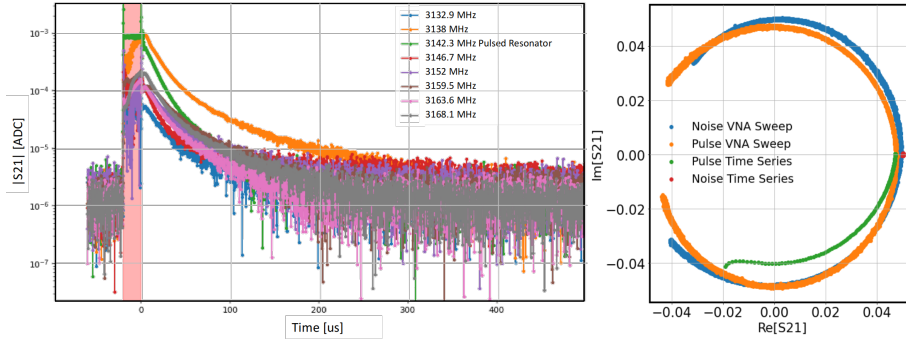


Fig. 2: *Left*: Driving a KID with a square pulse of  $> 10$  dBm readout power over a  $20 \mu\text{s}$  window (pink shaded region), in this case the 3142 MHz resonator (green line), results in quasiparticle production and subsequent absorption in neighboring resonators, much like a regular particle interaction. *Right*:  $S_{21}$  view of different datasets taken using the 3142 MHz resonator. The indicated pulse in this case was one received by pulsing another neighboring resonator.

### 3 Impedance mismatches and measuring quality factors

The actual transmission spectra of real devices, e.g. in Fig. 3 *Top*, shows deviations in the resonance circle from the expected transmission  $S_{21} = 1 - (Q_r/Q_c)/2jQ_r x$  (with  $x \equiv (f - f_r)/f_r$ ) at resonance for total quality factor  $Q_r$ , where  $Q_r^{-1} = Q_c^{-1} + Q_i^{-1}$ . These lead to an asymmetric line shape even at low-power. Khalil et al. [6] attribute this to an impedance mismatch between the input and output lines of the resonator. They quantify this by introducing an imaginary component to the coupling quality factor, parametrized by a rotation angle  $\phi$  and leading to a modified description of the transmission:

$$S_{21}(f) = a e^{-2\pi j f \tau} \left[ 1 - \frac{(Q_r/Q_c \cos \phi) e^{j\phi}}{1 + 2jQ_r x} \right] \quad (2)$$

where we have also included a complex feedline attenuation term  $a$ , a feedline delay term  $\tau$ , and  $f_r$  is the resonant frequency. Measuring individual terms in Eq. 2 is achieved by fitting to the raw transmission spectrum, as seen in Fig. 3 *Bottom*, and is potentially degenerate in solution. A related, but purely empirical way of estimating quality factors is by a) directly

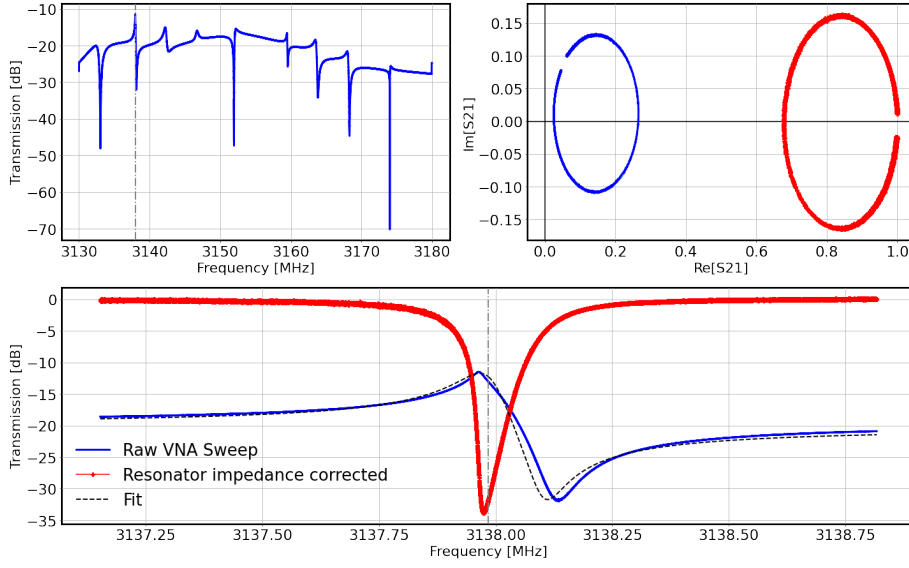


Fig. 3: *Top Left*: S21 Transmission across all studied resonators, showing the characteristics dips. Note the uneven overall level and upward spiking features. *Top Right, Bottom*: Resonance circles and transmission spectra of the 3138 MHz resonator before and after the impedance match corrections outlined by Khalil et al., showing the effect of the  $\phi$  rotation and scaling by  $\cos(\phi)$  (referenced in Eq. 2) to recovering the expected Lorentzian transmission feature of a resonator.

measuring the diameter of the resonance circle to evaluate  $Q_r/Q_c \cos \phi$ , and b) identifying the frequency direction of the resonance circle, knowing the readout frequency of each data point, and estimating  $\delta f_r/f_r \approx \delta x$ , extracting a quality factor ratio through:

$$\begin{aligned} \delta S_{21} &\sim \frac{Q_r^2}{Q_c \cos \phi} \left( \delta \frac{1}{Q_i} - 2j \frac{\delta f_r}{f_r} \right) \\ \implies \frac{Q_r^2}{Q_c \cos \phi} &\approx \frac{1}{2} \frac{\delta S_{21}}{\delta x} \end{aligned} \quad (3)$$

#### 4 Device Performance and Discussion

We can then use the M-B relations  $\delta(1/Q_i) \approx \alpha \kappa_1 n_{qp}$  and  $\delta f_r/f_r \approx -\alpha \kappa_2 n_{qp}/2$  [7], where  $\kappa_{1,2}$  are temperature sweep derived parameters that help us move to a quasiparticle number  $n_{qp}$  basis. So the final prescription is to compute the expected resolution using the raw noise and pulse data in the electronics basis from Eq. 1 and then use the empirically derived quality factors and measured transmission line parameters to convert  $\sigma_E$  to a quasiparticle basis. Fig. 4 shows the example of the  $\kappa_1$  direction energy resolution for various resonators at a -16 dBm readout power. As the *Left* plot shows, the resolution appears to be driven by differences in the quality factor ratio. Accounting for RF transmission and specifics of the pulse shape and noise spectrum, one can recover the expected linear relationship between the measured  $\sigma_{nqp}^{-2}$  and its constituent components. Looking at the  $Q_c$ ,  $Q_i$ , and  $\phi$  terms in

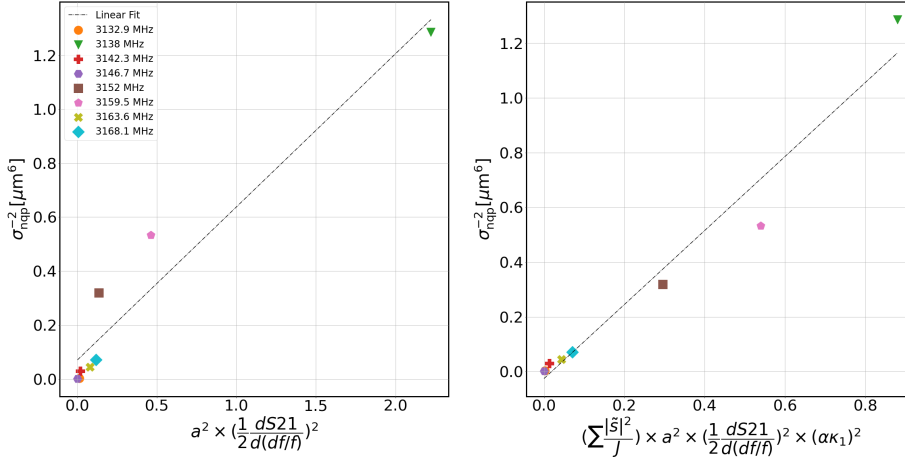


Fig. 4: Expected energy resolution from measurement in the  $\kappa_1$  direction at -16 dBm readout power, expressed in quasiparticle units, for the various studied resonators. *Left*: Resolution as related to the empirically measured  $Q^2/|Q_c|$ . Differences in this quantity appear to drive the variation in resolution. *Right*: Accounting for RF transmission, the defined x-axis quantity should be linearly equivalent to the variance of the measured energy and this relationship is clearly demonstrated in the data.

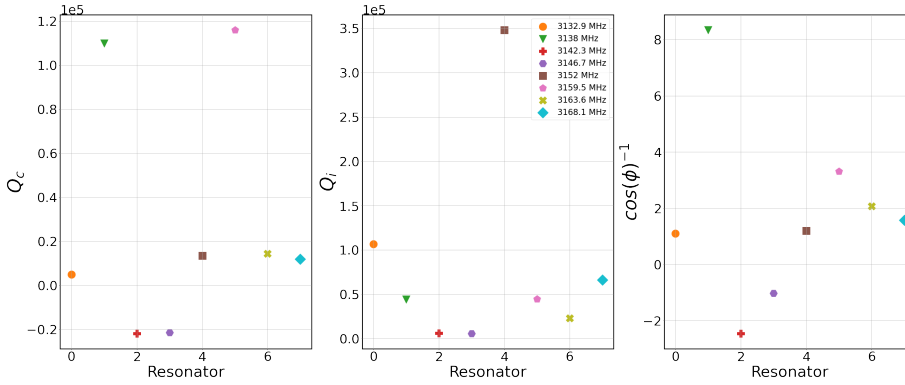


Fig. 5: Internal quality factor (*Left*), coupling quality factor (*Center*), and impedance mismatch  $\phi$  (*Right*), for all 8 studied resonators.

turn, as in Fig. 5, we note that the devices that show the greatest deviation from the pack, e.g. the 3138 MHz resonator, are the same ones that show the largest difference in resolution in Fig. 4. In addition we notice certain unexpected negative quantities for the coupling quality factor, though this is offset by a corresponding negative scaling term. Converting from a quasiparticle basis to a substrate deposited energy resolution, where we include the KID volume  $V$  and account for phonon to quasiparticle conversion efficiency via  $\eta_{\text{ph}} \approx 0.3$  we

have that the best and worst performing KIDs have a resolution of:

$$\begin{aligned} \sigma_{eV} &= \sigma_{nqp} \times \Delta \times V / \eta_{ph} & (4) \\ \implies \sigma_{best} &= (1.3)^{-2} \times 200 \mu eV \times 30000 \mu m / 0.3 \approx 16 eV \\ \sigma_{worst} &= (2000)^{-2} \times 200 \mu eV \times 30000 \mu m / 0.3 \approx 400 eV \end{aligned}$$

The currently unexplained differences in the quality factors, whether due to impedance

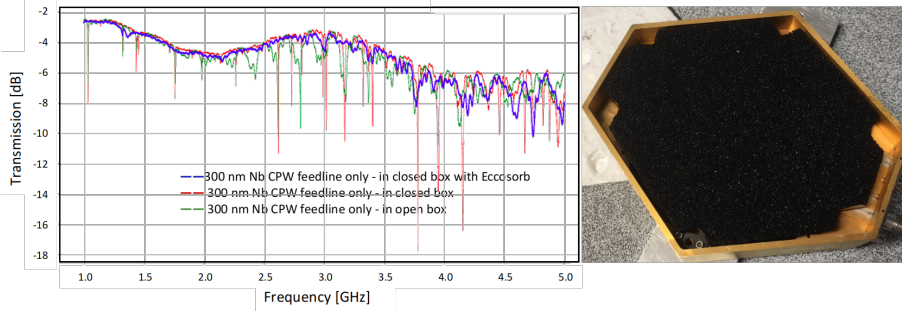


Fig. 6: *Left*: S21 transmission of a 300 nm wide Niobium CPW feedline for different physical configurations of the Cu box, as measured in a 4K fridge. *Right*: Holder lid with applied Eccosorb layer held on by circlips.

matching issues or inherent differences between resonators appear to drive the variation in measured energy resolution. One hypothesis for the observed behavior is the presence of box modes, i.e. electromagnetic coupling between the device and its metallic holder box, sourcing the changing performance. Some support for this hypothesis was established by measuring the transmission for a feedline only device, as seen in Fig. 6, in different physical configurations. In the closed box configuration (red line), one observes numerous spectral line features, indicative of these box modes. Other spectral features are apparent with the device lid off (green line), but these modes are completely removed after applying a thin  $\sim$ mm layer of Eccosorb dielectric foam absorber (blue line). However there is risk that this can degrade resonator quality factors, because the Eccosorb can remain at an elevated temperature and act like a blackbody load on the device.

## 5 Conclusion and Future Work

In this letter we have highlighted an ongoing concern in deploying large scale KID arrays, in that the energy resolution across devices is inconsistent even with identical designs. We used an empirical method to extract the quality factors for the resonators and were able to reconstruct the measured energy resolution from its constituent components. We briefly discussed a possible source of this variation as arising from box modes but accurately pinning it down will require further experimental testing and simulation. Eliminating the resolution variation between KIDs will be a necessary step towards deploying detectors with  $\mathcal{O}(100)$  KIDs and realizing the promise of  $\mathcal{O}(10)$  eV energy resolution necessary for future precise rare-event searches.

**Acknowledgements** We acknowledge the support of the following institutions and grants: NASA, NSTGRO 80NSSC20K1223; Department of Energy, DE-SC0011925F; Fermilab, LDRD Subcontract 672112

## References

1. P. K. Day et. al., *Nature* 425, 817 (2003) DOI:10.1038/nature02037
2. D. C. Moore et. al., *Appl. Phys. Lett.* 100, 232601 (2012) DOI:10.1063/1.4726279
3. Y.Y. Chang et. al., *Journal of Low Temp. Phys.* Vol. 193, pp 1199–1205 (2018) DOI:10.1007/s10909-018-1900-9
4. S. R. Golwala, Dissertation (Ph.D.), University of California at Berkeley (2000)
5. B. Cornell, Dissertation (Ph.D.), California Institute of Technology (2018)
6. M. S. Khalil et. al., *Journal of Appl. Phys.* 111, 054510 (2012) DOI:10.1063/1.3692073
7. J. Gao, Dissertation (Ph.D.), California Institute of Technology (2008)